A&A 482, 59–65 (2008)
DOI: 10.1051/0004-6361:20078960

Astronomy & Astrophysics

Ages and metallicities of circumnuclear star formation regions from Gemini IFU observations

O. L. Dors Jr.[1], T. Storchi-Bergmann[1], R. A. Riffel[1], and Alex. A. Schimdt[2]

[1] Universidade Federal do Rio Grande do Sul, IF, CP 15051, Porto Alegre 91501-970, RS, Brazil
e-mail: oli.dors@ufrgs.br
[2] Universidade Federal de Santa Maria, 97110-000 Santa Maria, RS, Brazil

Received 29 October 2007 / Accepted 28 January 2008

ABSTRACT

Aims. We derive the age and metallicity of circumnuclear star formation regions (CNSFRs) located in the spiral galaxies NGC 6951 and NGC 1097 and investigate the cause of the very low equivalent widths of emission lines found for these regions.
Methods. We used optical two-dimensional spectroscopic data obtained with Gemini GMOS-IFUs and a grid of photoionization models to derive the the metallicities and ages of CNSFRs.
Results. We find star formation rates in the range 0.002–0.14 $M_{\odot}$ yr^{-1} and oxygen abundance of $12 + \log(\mathrm{O/H}) \approx 8.8$ dex, similar to those of most metal-rich nebulae located in the inner region of galactic disks.
Conclusions. We conclude that the very low emission-line equivalent widths observed in CNSFRs are caused by the "contamination" of the continuum by (1) contribution of the underlying bulge continuum combined with (2) contribution from previous episodes of star formation at the CNSFRs.

Key words. Galaxy: abundances – ISM: abundances – ISM: HII regions – ISM: evolution – Galaxy: bulge

1. Introduction

The pioneer works by Morgan (1958) and Sérsic & Pastoriza (1967) have shown that many spiral galaxies host circumnuclear star formation regions (CNSFRs) and several works have studied these regions. In one of the most recent works, Knapen (2005) uses Hα images of a sample of spiral galaxies to study CNSFRs, as well as nuclear star formation regions. They found that CNSFRs are present in about 20% of spiral galaxies and almost always occur within a barred host. In this paper we adopt the definition of Knapen (2005) to distinguish CNSFRs from nuclear star formation regions: CNSFRs are the ones observed within circular areas with diameters of a few kpc around the galactic nucleus, while nuclear star formation regions are observed in more internal areas a few hundred parsec across. In particular, the formation of CNSFRs in barred galaxies seems to be due to the radial inflow of gas along bars to the galactic center (Roberts et al. 1979; Friedli & Benz 1995; Sakamoto et al. 1999; Sheth et al. 2005; Jogge et al. 2005). This gas is accumulated in a ring structure between two inner Lindblad resonances (Knapen et al. 1995).

Gas inflow is also necessary to feed the nuclear massive black hole in active galactic nuclei (AGNs) and surrounding nuclear star formation regions, probably yielding the so-called AGN-starburst connection (Norman & Scoville 1988; Terlevich et al. 1990; Heckman et al. 1997; González Delgado et al. 1998; Ferrarese & Merritt 2000; Cid Fernandes et al. 2001; Storchi-Bergmann 2001; Heckman 2004). Recent observational studies have shown evidence of gas inflow: Storchi-Bergmann et al. (2007) and Fathi et al. (2006) report the discovery of gas streaming motions along spiral arms towards the LINER nuclei of the galaxies NGC 6951 and NGC 1097, while Fathi et al. (2007) found gas inflow to the nuclear star formation region of the galaxy M 83. Moreover, several works have found star formation around active nuclei (e.g. Riffel et al. 2007; Kauffmann et al. 2003).

In CNSFRs, the line ratio [O III]λ5007/Hβ (hereafter [O III]/Hβ) is usually weak or not observable and the emission lines have lower equivalent widths than those of disk H II regions (e.g. Diaz et al. 2007; Bresolin et al. 1999; Bresolin & Kennicutt 1997; Kennicutt et al. 1989). The low value of [O III]/Hβ has been attributed to over-solar abundances (e.g. Boer & Schulz 1993). At their location in the innermost parts of galactic disks, these objects are expected to be the most metal-rich star-forming regions. In fact, Díaz et al. (2007) obtained long-slit observations for 12 CNSFRs and, using a semi-empirical method to derivate of oxygen abundances, found that some of them have $12 + \log(\mathrm{O/H}) = 8.85$, a value consistent with the maximum oxygen abundance value derived for central parts of spiral galaxies (Pilyugin et al. 2007).

Regarding the equivalent width of emission lines, Kennicutt et al. (1989) found that the equivalent widths of Hα EW(Hα) in CNSFRs are about 7 times lower than the ones in disk H II regions. They proposed several scenarios to explain this behavior, such as (i) deficiency of high-mass stars in the initial mass function (IMF), (ii) a long timescale for star formation, and (iii) high dust abundance. However, neither of these mechanisms turned out to be the dominant effect. Unfortunately, spectroscopic data and abundance estimates are only available for a small number of CNSFRs.

With the goal of increasing the number of CNSFRs with determined gas abundances and star formation rates, we have combined two-dimensional integral field unit (IFU) data of CNSFRs located in the galaxies NGC 1097 and NGC 6951 with a grid of photoionization models to derive their nebular gas properties. Using high-quality two-dimensional data, we could also investigate the cause of lower equivalent widths of emission lines observed in CNSFRs with respect to those of inner disk

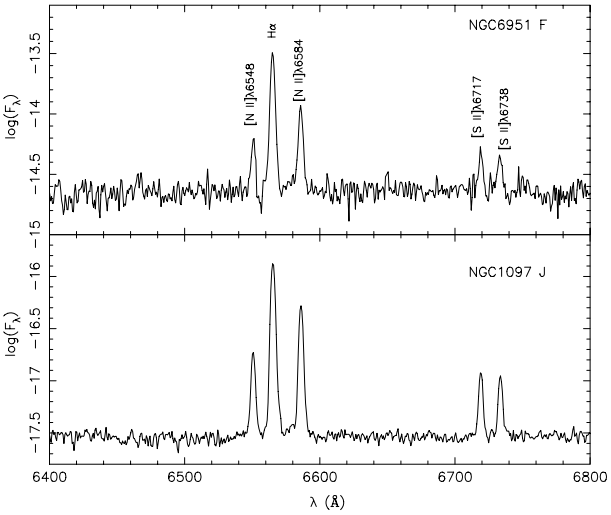

Fig. 1. Sample spectra: star-forming regions F in NGC 6951 (*top*) and *J* in NGC 1097 (*bottom*).

HII regions. In Sect. 2 we give details about the observational data we used, in Sect. 3 we present a description of the methodology used to derive the physical parameters, while in Sect. 4 we present our results. The discussion of the outcome and our final conclusions are given in Sects. 5 and 6, respectively.

2. Observational data

The observational spectroscopic data on NGC 1097 and NGC 6951 were drawn from the works of Fathi et al. (2006) and Storchi-Bergmann et al. (2007). Basically these data were obtained with IFUs of the Gemini Multi-Object Spectrographs (GMOS-IFU) on the Gemini South (for NGC 1097) and North (for NGC 6951) telescopes using the R400-G5325 grating and r-G0326 filter, covering the spectral range 5600–7000 Å with a resolution of $R \approx 2300$. Three IFU fields were observed in each galaxy, covering an angular field of $15'' \times 7''$. The reduction procedure resulted in 50×70 spectra for each IFU field, each corresponding to an angular coverage of $0.1'' \times 0.1''$. We adopted distances for NGC 6951 and NGC 1097 of 24 Mpc and 17 Mpc (Tully 1988), respectively, such that $1''$ corresponds to 96 pc for the former and 68 pc for the latter galaxy. The reader is referred to the papers above for a full description of the data.

Figure 1 shows spectra of CNSFRs identified by the letters *F* and *J* in Figs. 2 and 3 located in the circumnuclear rings of NGC 6951 and NGC 1097, respectively. Using the observed spectra we built maps for flux distributions in the Hα emission line and for the line ratios [N II]λ6583/Hα, ([S II]λ6717 + λ6731)/Hα, as well as for the EW(Hα). These maps are shown in Figs. 2 and 3. Throughout the paper we identify the line ratios above as [N II]/Hα and [S II]/Hα. For NGC 6951 the observed field completely covers the circumnuclear ring. The data of the ring were separated from those of the inner region by fitting two ellipses to the Hα image of NGC 6951: one to the inner border of the ring and the other to the outer border (see Storchi-Bergmann et al. 2007). In the NGC 6951 Hα map, we clearly see several regions of star formation. We have identified nine of them as indicated in Fig. 2. Since for NGC 1097 the observation field covered only part of the ring, we could only identify two regions in this galaxy (see Fig. 3).

For these measurements, we assumed that each star formation region has a circular symmetry, whose center corresponds to the peak in the Hα intensity and the radius defined as the one where the flux reaches 50% of the peak value. Nevertheless, we can see from Fig. 2 that the CNSFRs have irregular morphologies and the assumption above can result in some uncertainties in the Hα flux and in line ratio measurements. To estimate how much flux we may be missing, for NGC 6951, we compared the sum of the Hα flux of all regions (obtained from photometry within circular apertures) with the flux integrated over the whole ring. We found that the diffuse gas contribution (from regions not covered by the circles) is about 12%. A similar result was found for individual H II regions by Oey & Kennicutt (1997). In relation to line ratios, we measured the median values considering different values for the radius of each region and differences no greater than 10% were found. We thus estimate that uncertainties in both fluxes and line ratios due to uncertainties in the geometry of the CNSFRs are about 10%. In Table 1 we show the adopted area of each region, the luminosity of Hα, and the median values of EW(Hα), [N II]/Hα, and [S II]/Hα.

3. Photoionization models

To derive the metallicity, ionization parameter, and the age of the CNSFRs, we employed the photoionization code Cloudy/95.03 (Ferland 2002) to build a grid of models covering a large space of nebular parameters. The models were built as in Dors & Copetti (2006), with metallicities $Z = 1.1$, 1.0, 0.7, 0.6 $Z_\odot$, and ionization parameter logarithm ($\log U$) of -2.0, -2.5, and -3.0 dex. In each model a stellar cluster was assumed as the ionizing source with the stellar energy distributions obtained from the synthesis code *STARBURST*99 (Leitherer et al. 1999). We built models with stellar clusters formed by instantaneous and continuous bursts with stellar upper mass limits of $M_{\rm up} = 20$, 30 and 100 $M_\odot$, $Z = 1.0$ and 0.4 $Z_\odot$, and ages ranging from 0.01 to 10 Myr with a step of 0.5 Myr. Clusters older than about 10 Myr and formed instantaneously have no more O stars (Leitherer & Heckman 1995), so were not considered in our models. The metallicity of the nebula was matched to the closest available metallicity of the stellar cluster. The solar composition refers to Asplund et al. (2005) and corresponds to $\log(\mathrm{O/H}) = -3.30$.

4. Results

Since the observational data for NGC 6951 and NGC 1097 covers a restricted wavelength range, few emission line ratios can be used in our analysis. Storchi-Bergmann et al. (1994) and Raimann et al. (2000) showed that [N II]/Hα can be used to obtain the oxygen abundance of star-forming galaxies. However, this line ratio also dependents on the ionization parameter U (Kewley & Dopita 2002), thus the combination with other line ratios is desirable in order to decrease the uncertainties in the O/H estimates. Thus we used our photoionization model grid to build an [N II]/Hα vs. [S II]/ Hα diagram to derive Z and U of the CNSFRs located in NGC 6951 and NGC 1097. Recently, Viironen et al. (2007) have shown that diagnostic diagrams using [N II]/Hα and [S II]/ Hα are a powerful tool for estimating Z and U of star-forming regions. Moreover, these line ratios are not dependent on the $M_{\rm up}$ and age assumed in the models (see Fig. 5). We point out that a cautionary note has been put forth by Mazzuca et al. (2006) regarding the use of diagnostic diagrams including the line ratio [N II]/Hα: they can yield degenerate values for the metallicity, as star-forming regions with low Z and U have [N II]/Hα values similar to regions with high Z and U. However, CNSFRs are known to have high abundances (near solar) (see Sect. 5.1), ruling out the possibility of low abundances.

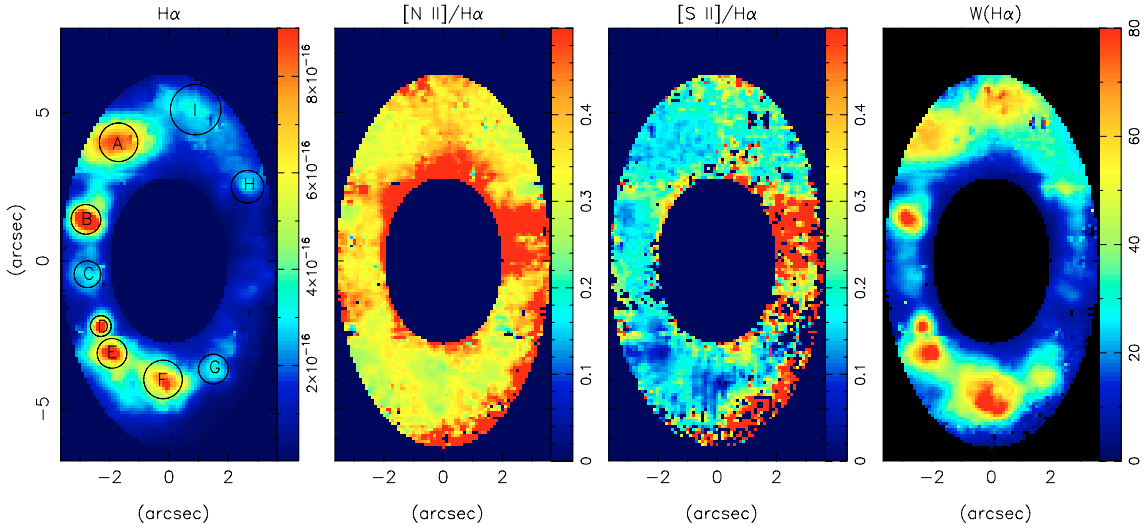

Fig. 2. Star-forming ring in NGC 6951. *From left to right*: map of the Hα integrated flux (erg cm^{-2} per pixel); line ratio maps [N II]/Hα [S II]/Hα and EW(Hα). The circles and the letters identify each region as defined in Sect. 2.

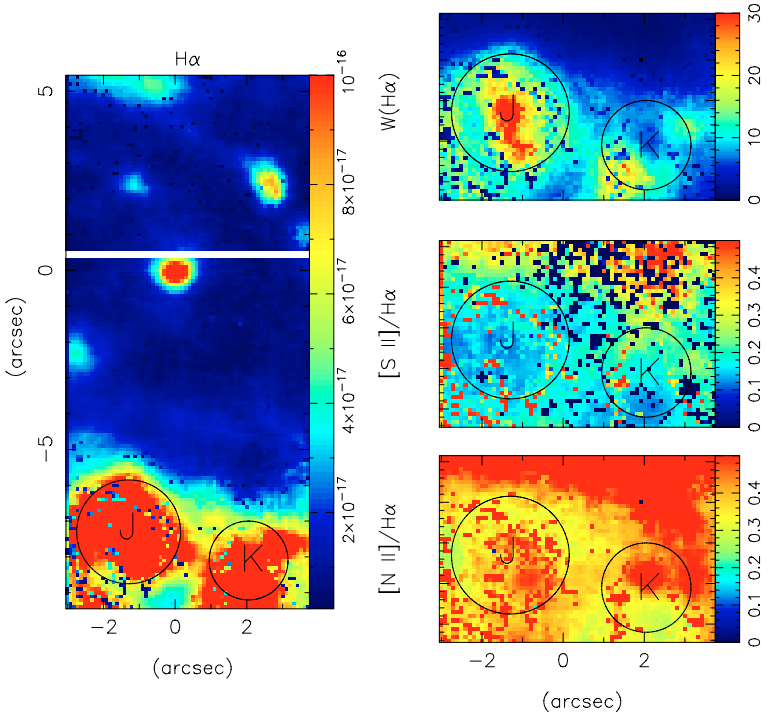

Fig. 3. *Left*: map of the Hα-integrated flux (erg cm^{-2} per pixel) showing the field covered by the IFU in NGC 1097, which includes the nucleus and part of the ring (at the bottom). *Right*: line ratio maps [N II]/Hα [S II]/Hα and EW(Hα) for the partial ring. The circles and the letters identify each region defined in Sect. 2.

This is confirmed by the work of Storchi-Bergmann et al. (1996), which shows an increasing gas abundance towards the nucleus, including a few regions in circumnuclear rings.

The results of our models compared to observational data for NGC 6951 and NGC 1097 are shown in Fig. 4, in which we considered an instantaneous burst with age of 2.5 Myr and $M_{\rm up}$ = 100 $M_{\odot}$. We can see that the observational data are well represented by models having metallicities $Z \approx Z_{\odot}$ and $\log U \approx -2.3$, with uncertainties of about 0.03 and 0.1 dex, due to the uncertainties in the line ratios discussed above. In Table 1 we show the Z and $\log U$ values for each region, obtained by linear interpolation from the model grid. In this table we also present the values of electron density $N_{\rm e}$ computed from the observed line ratio [S II]λ6717/λ6731 and adopting $T_{\rm e} = 10^4$ K (Osterbrock 1989). The $N_{\rm e}$ values cover the range 50–600 cm^{-3}, which is typical of H II regions (Copetti et al. 2000).

To obtain the ages of the CNSFRs, we used the observed values of equivalent widths and [O III]/Hβ, which decrease almost monotonically as a function of time (Magris et al. 2003; Copetti et al. 1986). In Fig. 5 we plot the values predicted by the models for EW(Brγ), EW(Hβ), EW(Hα), as well as [N II]/Hα, [S II]/Hα and [O III]/Hβ versus age. We considered instantaneous and continuous star formation bursts with $M_{\rm up}$ = 20, 30 and 100 $M_{\odot}$, $\log U = -2.5$ and $Z = Z_{\odot}$. The values of the line ratios [N II]/Hα and [S II]/Hα were found to be approximately constant for the range of ages considered. However, [O III]/Hβ shows a chaotic behavior between 2 and 6 Myr, mainly for $M_{\rm up}$ = 100 $M_{\odot}$ and instantaneous burst. This happens due to the increase in the number of ionizing photons by the presence of Wolf Rayet stars in this phase (Leitherer & Heckman 1995). This behavior was also noted by Dopita et al. (2006). As no feature of Wolf Rayet stars was observed in our data and because [O III]/Hβ is very

Table 1. Physical properties of the CNSFRs in NGC 6951 and NGC 1097.

Region	A (arcsec^2)	$L_{H\alpha}$ (10^{38} erg s^{-1})	[N II]/Hα	[S II]/Hα	SFR ($M_\odot$ yr^{-1})	EW(Hα)	$Z/Z_\odot$	log U	N_e (cm^{-3})
A	3.0	121	0.32 ± 0.03	0.15 ± 0.01	0.09	28	1.04	−2.3	208 ± 59
B	1.5	68.2	0.35 ± 0.03	0.16 ± 0.01	0.05	31	1.05	−2.2	287 ± 151
C	1.4	23.1	0.35 ± 0.03	0.18 ± 0.01	0.02	16	1.04	−2.4	297 ± 134
D	0.6	25.0	0.31 ± 0.02	0.15 ± 0.01	0.02	39	1.03	−2.3	525 ± 103
E	1.4	59.7	0.32 ± 0.02	0.13 ± 0.01	0.05	45	1.05	−2.1	354 ± 24
F	2.9	94.5	0.29 ± 0.01	0.11 ± 0.02	0.07	26	1.04	−2.0	148 ± 40
G	0.9	16.5	0.31 ± 0.01	–	0.01	32	–	–	273 ± 36
H	0.8	12.2	0.34 ± 0.02	0.22 ± 0.02	0.01	31	0.94	−2.6	68 ± 10
I	3.0	47.6	0.34 ± 0.02	0.20 ± 0.01	0.04	38	0.99	−2.6	138 ± 29
J	8.9	45.8	0.38 ± 0.02	0.16 ± 0.01	0.03	12	1.08	−2.1	292 ± 45
K	1.8	2.06	0.40 ± 0.03	0.18 ± 0.01	0.002	7	1.09	−2.2	223 ± 149

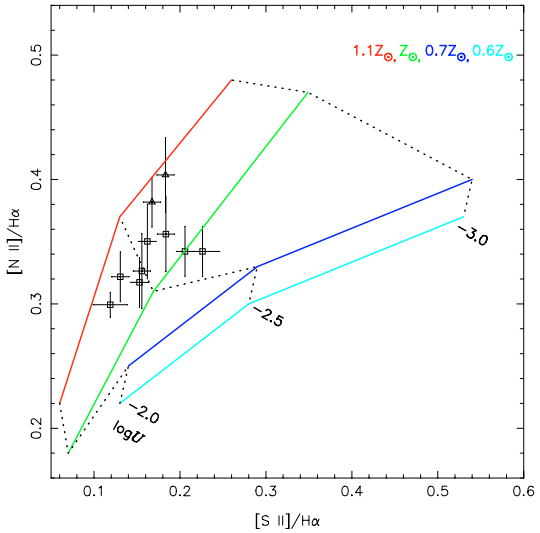

Fig. 4. Diagnostic diagram [N II]/Hα vs. [S II]/Hα showing the grid of photoionization models for an ionizing cluster with age 2.5 Myr and M_{up} = 100 $M_\odot$. Solid lines connect curves of iso-Z, while dotted lines connect curves of iso-U. The values of log U and Z are indicated. Squares are the median values measured for the CNSFRs in NGC 6951 and triangles are those for NGC 1097.

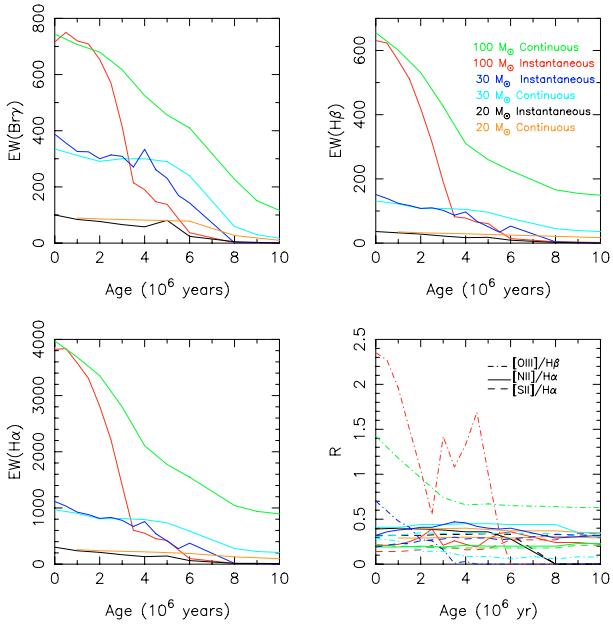

Fig. 5. Evolution of the EW(Brγ), EW(Hβ), EW(Hα), and relevant line ratios as predicted by our photoionization models considering different M_{up} values and star formation regimes as indicated, for $Z = Z_\odot$ and log $U = -2.5$.

dependent on many nebular parameters, it will not be considered as an age tracer in this paper. The use of the equivalent width of emission lines seems to be more reliable for deriving ages of star-forming regions, since they basically depend on M_{up} and on the slope of the IMF (Copetti et al. 1986).

Using the EW(Hα) values shown in Table 1, the CNSFR ages predicted by instantaneous and continuous models are around 7 Myr and over 10 Myr, respectively, independent of the M_{up} assumed. Table 1 also presents the values for the star formation rate (SFR) computed using the luminosity of the regions obtained in this paper and the relation $SFR(M_\odot\ \text{year}^{-1}) = 7.9 \times 10^{-42} L(\text{H}\alpha)$ (erg s^{-1}) given by Kennicutt (1998).

5. Discussion

5.1. Metallicities

Acording to our models, the CNSFRs of NGC 6951 and NGC 1097 have solar or slightly higher solar metallicities. Considering an uncertainty on the order of 0.1 dex due to the method used to estimate abundances (see Evans 1986; Dors & Copetti 2005, 2006), our abundance values are comparable to the maximum oxygen abundance derived for central parts of spiral galaxies of $12 + \log(\text{O/H}) \approx 8.87$ (Pilyugin et al. 2007). Similarly, Mazzuca et al. (2006) present an emission-line diagnostic analysis of the nuclear starburst ring of NGC 7742 and find roughly solar abundances.

Recently, Sarzi et al. (2007) presented a study of CNSFRs located in eight galaxies which include the regions B, E and F of our sample. They also used empirical methods to derive the metallicities of these regions and find abundances similar to the ones derived in this paper. Díaz et al. (2007) use a semi-empirical abundance calibration to find that the CNSFRs in NGC 2903, NGC 3351, and NGC 3504 have metallicities comparable to the ones derived in this paper. Until now, only a case of very low abundance on the order of 0.2–0.4 $Z_\odot$ in the CNSFRs located in NGC 3310 was reported by Pastoriza et al. (1993). This low abundance can be understood as due to the fact that this galaxy has an interaction history (Elmegreen et al. 2002), through which neutral gas may have been accreted to the ring.

Due to the fact that CNSFRs have very low excitation, with [O III]/Hβ < 1 (e.g. Hägale et al. 2007; Pérez et al. 2000) and to their central location in the galactic disk, it is expected that these

objects have somewhat higher abundance than is derived for inner disk H II regions. To check this, we have plotted the [N II]/Hα in Fig. 6 (lower panel) against oxygen abundance for some disk H II regions located in 13 spiral galaxies. This sample includes the most metal-rich nebulae in which temperature sensitive emission lines have been detected. The data were taken from Bresolin (2007), Bresolin et al. (2005, 2004), Kennicutt et al. (2003), Castellanos et al. (2002), and Skillman et al. (1996). With the exception of the oxygen abundances from Skillman et al. (1996), which were recalculated by us using the *P*-method (Pilyugin 2001), all O/H values were obtained using direct derivation of the electron temperature. Also included in Fig. 6 are the data of our sample. We can see that the CNSFRs show the highest oxygen abundances, together with some disk nebulae, a result also obtained by Díaz et al. (2007). Since abundance determinations via photoionization models are overestimated by a factor of 0.1–0.4 dex when compared to direct determinations (Dors & Copetti 2005), our abundance estimates should be interpreted as upper limits. If CNSFRs are included in the computation of abundance gradients in spirals, we would expect therefore a plateau at very small galactocentric distances.

5.2. Star formation history

The Hα luminosity values found for the CNSFRs in this paper are in the range 2×10^{38}–1.2×10^{40} erg s^{-1}, compatible with values of regions in circumnuclear rings of other spiral galaxies (e.g. Díaz et al. 2007). These luminosity values yield star formation rates of 0.002–0.1 $M_{\odot}$ yr^{-1}, characterizing a moderate star-forming regime. Averaging the SFR values in Table 1, we find 0.04 $M_{\odot}$ yr^{-1}, a similar value to the one found by Ho et al. (1997) for a sample of nuclear star-forming regions and by Shi et al. (2006), who studied a sample of 385 circumnuclear star-forming regions in galaxies with different Hubble types.

We cannot conclude from our data alone whether the star formation has been continuous or instantaneous in the rings, although the former scenario has not been favored by previous studies. For example, Sarzi et al. (2007) use absorption-line index diagrams to show that the hypothesis of a constant star formation in their sample can be ruled out. Allard et al. (2006) find that the star formation in the ring of M 100 have occurred in a series of short bursts for the past 500 Myr or so. These results can be understood within the following scenario. Once massive stars are formed, they cause turbulence and heating in the molecular cloud, inhibiting further star formation (Hartmann et al. 2001; Blitz & Shu 1980). Since no systematic age sequence is observed along the NGC 6951 ring, the star formation mode seems to be as predicted by the *popcorn model* (Böker et al. 2008), in which the entire ring begins to form stars at about the same time or at random times. A similar result was also derived by Mazzuca et al. (2008), who used photometric Hα imaging of 22 nuclear rings to find that only a very small fraction of them show age sequences along the ring.

5.3. Age estimates

Our modeling gives ages of about 7.0 Myr for an instantaneous burst and more than 10 Myr for a continuous burst, with the CNSFRs in NGC 1097 slightly older than in NGC 6951. To compare our age estimates with those of other CNSFRs, we collected equivalent widths of more CNSFRs from the literature and estimated their ages using Fig. 5. The data were extracted from Díaz et al. (2007) for NGC 2903 and NGC 3505, Hägele et al. (2007) for NGC 3351, Allard et al. (2006) for M 100, Reunanen et al. (2000) for NGC 7771, and Wakamatsu & Nishida (1980) for NGC 4314, which give EW(Hβ), EW(Hα), and EW(Brγ) in the range 1–17, 10–40, and 5–60 Å, respectively. The predicted ages for these EW values are of 5–8 Myr and more than 10 Myr for instantaneous and continuous bursts, respectively, thus similar to the ones we derived for the CNSFRs in the present paper. Somewhat higher EW values have been obtained by Mazzuca et al. (2008) for HII regions in nuclear rings of more than 20 galaxies. On the other hand, studies also utilizing photoionization models give ages of 1.5–3 Myr for H II regions located in galactic disks and for H II galaxies (Dors & Copetti 2006; Stasinska & Izotov 2003; Bresolin et al. 1999; Copetti et al. 1985). We have also compared the ages of our sample with those of disk nebulae of similar metallicity. In Fig. 6 we show log(EW(Hβ)) and 12 + log(O/H) plotted against log([N II]/Hα) for these disk H II regions, together with our data for the CNSFRs. We converted the EW(Hα) values shown in Table 1 in EW(Hβ) using the relation $EW(\mathrm{H}\beta) \approx 0.15\ EW(\mathrm{H}\alpha)$ obtained from our models. We can see that the EW(Hβ) of the CNSFRs are lower by a factor of about 30 than those of their counterpart disk H II regions. Assuming a $EW(\mathrm{H}\beta) = 100$ Å for the innermost disk regions and using Fig. 5, we find that these regions are about 3 Myr younger than the CNSFRs.

5.4. The low EW values

The age differences found above may not be real, since the very low equivalent widths in CNSFRs stem from other effects than the age. Kennicutt et al. (1989) pointed out possible mechanisms such as (i) deficiency of high-mass stars in the initial mass function, (ii) very high dust abundance, (iii) contamination of the continuum by contribution from the bulge or other underlying stellar populations, and (iv) continuous star formation. These hypotheses are discussed below.

Regarding the hypothesis of the deficiency of high-mass stars, since M_{up} of an ionizing cluster is dependent on the metallicity (Larson & Starrfield 1971; Kahn 1974; Shields & Tinsley 1976; Stasińska 1980; Vilchez & Pagel 1988; Campbell 1988; Bresolin et al. 1999; Dors & Copetti 2003, 2005, 2006), CNSFRs and innermost disk nebulae should have about same M_{up}. It is unlikely that the discrepancy in EWs is only due to variation in M_{up}. Even assuming that the ionizing cluster of disk nebulae have $M_{\mathrm{up}} = 100\ M_{\odot}$ and the ones of CNSFRs have $M_{\mathrm{up}} = 20\ M_{\odot}$, the age difference remains. Also a variation in the IMF can be discarded, since stellar clusters appear to form with a universal IMF slope (Kroupa 2007, 2002; Chabrier 2003).

The hypothesis of very high dust abundance in CNSFRs is not favored because they have similar Balmer decrements to those observed for disk H II regions, suggesting that this is not the main source of the low EWs in CNSFRs (Kennicutt et al. 1989).

Concerning the contamination of the continuum, several works have found the presence of underlying stellar populations from previous generations of stars in CNSFRs, which can decrease the equivalent widths and yield no real age estimates from Fig. 5. For example, Buta et al. (2000) found a spread in ages of about 5 to 200 Myr for clusters in the circumnuclear ring of NGC 1326, with the largest number of clusters younger than 20 Myr. In the case of NGC 6951 and with measurements of the equivalent width of calcium triplet at ≈8500 Å, Pérez et al. (2000) found evidence of a population of red supergiant stars with ages of 10 to 20 Myr in the ring.

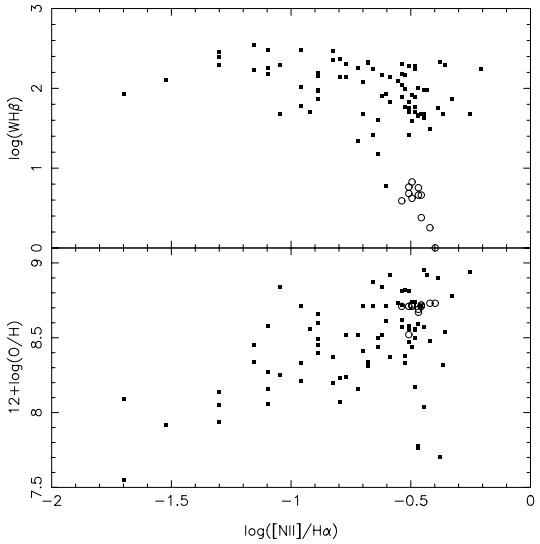

Fig. 6. Oxygen abundance vs. [N II]/Hα (*lower panel*) and *EW*(Hβ) vs. [N II]/Hα (*upper panel*). The squares represent data collected from the literature, while the circles represent the data of the CNSFRs analyzed in this paper.

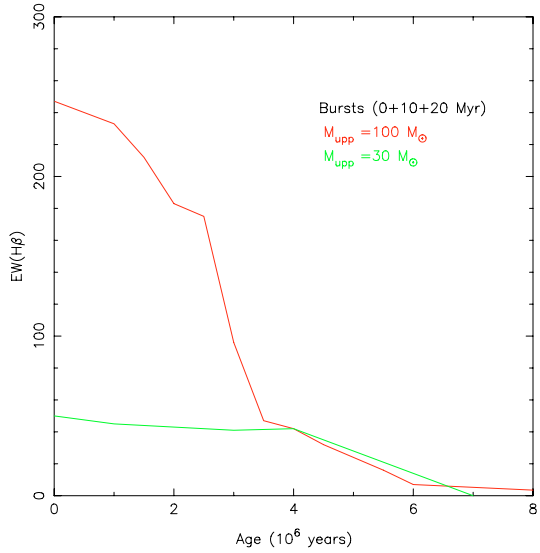

Fig. 7. Evolution of the *EW*(Hβ) as predicted by photoionization models considering three episodes of star formation as indicated. The ages correspond to the youngest burst.

An underlying stellar population can contribute in two ways to the low *EW*s by causing a Balmer absorption and yielding an extra contribution to the continuum. To estimate the effect of an underlying Balmer absortion, we constructed models of stellar populations (using the *Padova 1994 tracks*) with ages in the range 10–1000 Myr. We normalized the continuum of each model to the observed one and subtracted them from the observed spectra of the CNSFRs of NGC 6951. For all cases, the increase in the *EW* values due to subtracting of an underlying absorption was at most 10%, much less than needed to compensate for the low observed *EW* in CNSFRs.

Determining of the continuum contribution from underlying stellar populations is not an easy task, since two types of stellar populations can be contributing: the stellar population from the bulge and stars formed in previous episodes of star formation in the ring. To evaluate the contribution of the underlying bulge, we performed aperture photometry on the continuum images (not shown) measuring both the CNSFR continuum and that of the bulge in the surrounding regions. We concluded that the bulge contributes with ≈75% of the total flux in the case of NGC 6951 and with 50% in NGC 1097. The corresponding corrections are an increase by a factor of 2 and 4 in *EW*(Hα) for NGC 1097 and NGC 6951, respectively. These factors increase the *EW*(Hα) in NGC 6951 from average values of ≈30 Å to ≈120 Å and from ≈10 Å to ≈20 Å in NGC 1097. The corresponding changes in age are from ≈7 Myr to ≈6 Myr in NGC 6951 and no change for NGC 1097 (≈7 Myr). Thus the contribution from the bulge to the continuum also does not explain the low *EW*'s in CNSFRs. Stauffer (1981) also studied the bulge contamination using aperture photometry of galaxy nuclei to measure the background contribution to the continuum flux, and Kennicutt et al. (1989) used those results to find a correction factor similar to the one found by us.

Several generations of stars may coexist in CNSFRs because the tidal effects are not strong enough to disrupt the cluster at the radius of the ring, allowing several generations of stars to coexist (Buta et al. 2000). Thus the continuum may have a contribution from previous bursts of star formation in the rings. To investigate the effect of this continuum, we built photoionization models to represent a scenario where three bursts of star formation have occurred, with ages of 0.01, 10, and 20 Myr for two values of $M_{\rm up}$: 100 and 30 $M_{\odot}$. This is illustrated in Fig. 7, which shows the evolution of *EW*(Hβ) as a function of time. It can be seen that the *EW* values decrease considerably when compared with those of a single burst (Fig. 5). If we consider a typical *EW*(Hβ) for CNSFRs of 10 Å (not corrected for the underlying bulge contribution) and compute the age from Fig. 7, we find ages of 6–7 Myr, similar to the values derived above.

We conclude that none of the mechanisms discussed above alone yield the low *EW* values (and resulting larger age) observed in CNSFRs when compared to disk H II regions. However, it could be that a combination of more than one mechanism can explain the lower *EW*s in CNSFRs. For example, we can consider the effects of both the dilution by the bulge and by previous bursts of star formation. A typical *EW*(Hβ) = 10 Å in NGC 6951 will increase to 40 Å if we correct for contamination by the bulge. Then, we can consider the effect of previous generation of stars in the ring using Fig. 7 instead of Fig. 5 to obtain the age. We obtain an age of 3–4 Myr, a value in consonance with ages of the innermost disk regions. In this way we eliminate the apparent difference in age between CNSFRs and inner-disk H II regions.

6. Conclusions

We have used optical IFU spectroscopic data of CNSFRs in NGC 6951 and NGC 1097, which compared to a grid of photoionization models, in order to obtain physical parameters of these regions. We find that the star formation rates are in the range 0.002–0.14 $M_{\odot}$ yr^{-1}, thus covering a range from very low to moderate star-forming regime. We also find that the CNSFRs have oxygen abundances of 12 + log(O/H) ≈ 8.8, similar to those of the most metal-rich nebulae located in inner parts the disks of spiral galaxies.

We investigated the cause of the very low equivalent width of emission lines found in CNSFRs, which suggests an older age for these objects than for disk H II regions. Among the several scenarios invoked to explain this fact, we have concluded that the contamination of the continua of CNSFRs

by underlying contributions from both old bulge stars and stars formed in the ring in previous episodes of star formation (10–20 Myr) yield the observed low equivalent widths. Correcting for these contributions, there are not any more significant differences in ages between the CNSFRs and inner disk H II regions.

Acknowledgements. We thank the anonymous referee for valuable suggestions which helped to improve the paper. This work was based on observations obtained at the Gemini Observatory, which is operated by the Association of Universities for Research in Astronomy, Inc., under a cooperative agreement with the NSF on behalf of the Gemini partnership: the National Science Foundation (United States), the Science and Technology Facilities Council (United Kingdom), the National Research Council (Canada), CONICYT (Chile), the Australian Research Council (Australia), CNPq (Brazil) and SECYT (Argentina).

References

Allard, E. L., Knapen, J. H., Peletier, R. F., & Sarzi, M. 2006, MNRAS, 371, 1087
Asplund, M., Grevesse, & N., Sauval, A. J. 2005, Cosmic Abundances as Records of Stellar Evolution and Nucleosynthesis, The Solar Chemical Composition, ASP Conf. Ser., 336, 25
Boer, B., & Schulz, H. 1993, A&A, 277, 397
Böker, T., Falcón-Barroso Schinnerer, E., Knapen, J. H., & Ryder, S. 2008, AJ, 135, 479
Blitz, L., & Shu, F. H. 1980, ApJ, 238, 148
Bresolin, F. 2007, ApJ, 656, 186
Bresolin, F., & Kennicutt, R. C 1997, AJ, 113, 3
Bresolin, F., Kennicutt, R. C., & Garnett, D. R. 1999, ApJ, 510, 104
Bresolin, F., Garnett, D. R., & Kennicutt, R. C. 2004, ApJ, 615, 228
Bresolin, F., Schaerer, D., González Delgado, R. M., & Stasínska, G. 2005, A&A, 441, 981
Buta, R., Treuthardt, P. M., Byrd, G. G., & Crocker, D. A. 2000, AJ, 120, 1289
Campbell, A. 1988, ApJ, 335, 644
Castellanos, M., Díaz, A. I., & Terlevich, E. 2002, MNRAS, 329, 315
Chabrier, G. 2003, PASP, 115, 763
Copetti, M. V. F., Pastoriza, M. G., & Dottori, H. A. 1985, A&A, 152, 427
Copetti, M. V. F., Pastoriza, M. G., & Dottori, H. A. 1986, A&A, 156, 111
Copetti, M. V. F., Mallmann, J., Schmidt, A. A., & Castañeda, H. O. 2000, A&A, 357, 621
Cid Fernandes, R., Heckman, T., Schimitt, H., Gonzáles Delgado, R., & Storchi-Bergmann, T. 2001, MNRAS, 558, 81
Díaz, A. I., Terlevich, E., Castellanos, M., & Hägele, G. 2007, MNRAS, 382, 251
Dors, O. L., & Copetti, M. V. F. 2003, A&A, 404, 969
Dors, O. L., & Copetti, M. V. F. 2005, A&A, 437, 837
Dors, O. L., & Copetti, M. V. F. 2006, A&A, 452, 437
Dopita, M. A., Fischera, J., Sutherland, R. S., et al. 2006, ApJS, 167, 177
Elmegreen, D. M., Chromey, F., McGrath, E., & Ostenson, J. 2002, AJ, 123, 1388
Evans, I. N. 1986, ApJ, 309, 544
Hägele, G. F., Díaz, A. I., Cardaci, M. C., Terlevich, E., & Terlevich, R. 2007, MNRAS, 378, 163
Hartmann, L., Ballesteros-Paredes, J., & Bergin, E. A. 2001, ApJ, 562, 852
Heckman, T. M. 2004, cbhg. Symp, 358
Heckman, T. M., González Delgado, R. M., Leitherer, C., et al. 1997, ApJ, 482, 114
Ho, L. C., Filippenko, A. V., & Sargent, W. L. W. 1997, 487, 591
Fathi, K., Storchi-Bergmann, T., Riffel, R. A., et al. 2006, ApJ, 641, L25
Fathi, K., Beckman, J. E., Lundgren, A. A., et al. 2007 [arXiv:0712.0793]
Ferland, G. J. 2002, Hazy, a brief introduction to Cloudy 96.03, Univ. Kentucky, Dept. Phys., Astron. internal report
Ferrarese, L., & Merritt, D. 2000, ApJ, 539, L9
Friedli, D., & Benz 1995, A&A, 301, 649
González Delgado, R. M., Heckman, T., Leitherer, C., et al. 1998, ApJ, 505, 174
Jogge, S., Scoville, N., & Kenney, J. D. P. 2005, ApJ, 630, 837
Kahn, F. D. 1974, A&A, 37, 149
Kauffmann, G., Heckman, T. M., Tremonti, C., et al. 2003, MNRAS, 346, 1055
Kennicutt, R. C. 1998, ARA&A, 36, 189
Kennicutt, R. C., Keel, W., & Blaha, C. A. 1989, ApJ, 97, 1022
Kennicutt, R. C., Bresolin, F., & Garnett, D. R. 2003, ApJ, 591,
Kewley, L. J., & Dopita, M. A. 2002, ApJSS, 142, 35
Knapen, J. H. 2005, A&A, 429, 141
Knapen, J. H., Beckman, J. E., Heller, C. H., Shlosman, I., & de Jong, R. S. 1995, ApJ, 454, 623
Kroupa, P. 2002, Science, 295, 82
Kroupa, P. 2007 [arXiv:astro-ph/0703282]
Larson, R. B., & Starrfield, S. 1971, A&A, 13, 190
Leitherer, C., & Heckman, T. M. 1995, ApJS, 96, 9
Leitherer, C., Schaerer, D., Goldader, J. D., et al. 1999, ApJS, 123, 3
Magris, C. G., Binette, L., & Bruzual, A. G. 2003, ApJS, 149, 313
Mazzuca, L. M., Sarzi, M., Knapen, J. H., Veilleux, S., & Swaters, R. 2006, ApJ, 649, L79
Mazzuca, L. M., Knapen, J. H., Veilleux, S., & Regan, M. W. 2008, ApJS, 174, 337
Morgan, W. W. 1958, PASP, 70, 364
Norman, C., & Scoville, N. 1988, ApJ, 332, 124
Oey, M. S., & Kennicutt, R. C. 1997, MNRAS, 291, 827
Osterbrock, D. E. 1989, Astrophysics of Gaseous Nebulae and Active Galactic Nuclei (Mill Valley: Univ. Science Books)
Pastoriza, M. G., Dottori, H. A., Terlevich, E., & Terlevich, R. 1993, MNRAS, 260, 177
Pérez, E., Márquez, I. M., Durret, F., et al. 2000, A&A, 353, 893
Pilyugin, L. S. 2001, A&A, 369, 594
Pilyugin, L. S., Thuan, T. X., & Vílchez, J. M. 2007, MNRAS, 376, 353
Terlevich, E., Diaz, A. I., & Terlevich, R. 1990, MNRAS, 242, 271
Tully, R. B. 1988, Nearby Catalogue (Cambridge University Press)
Raimann, D., Storchi-Bergmann, T., Bica, E., Melnick, J., & Schmitt, H. 2000, MNRAS, 316, 559
Reunanen, J., Kotilainen, J. K., Laine, S., & Ryder, S. D. 2000, ApJ, 529, 853
Riffel, R., Pastoriza, G., Rodrígues-Ardila, A., & Maraston, C. 2007, ApJ, 659, L103
Riffel, R. A., Storchi-Bergmann, T., Winge, C., & Barbosa, F. K. 2006, MNRAS, 373, 2
Roberts, W. W., Huntley, J. M., & van Albada, G. D. 1979, ApJ, 233, 67
Sakamoto, K., Okumura, S. K., Ishizuki, S., & Scoville, N. Z. 1999, ApJ, 525, 691
Sarzi, M., Allard, E. L., Knapen, J. H., & Mazzuca, L. M. 2007, MNRAS, 380, 949
Stauffer, J. P. 1981, Ph.D. Thesis, University of California, Berkeley
Stasińska, G. 1980, A&A, 84, 320
Sérsic, J. L., & Pastoriza, M. 1967, PASP, 79, 427
Sheth, K., Vogel, S. N., Regan, M. W., et al. 2005, ApJ, 632, 217
Shields, G. A., & Tinsley, B. M. 1976, ApJ, 203, 66
Shi, L., Gu, Q. S., & Peng, Z. X. 2006, A&A, 450, 15
Skillman, E. D., Kennicutt, R. C., Shields, G. A., & Zaritsky, D. 1996, ApJ, 462, 147
Stasińska, G., & Izotov, I. 2003, A&A, 397, 71
Storchi-Bergmann, T., Calzetti, D., & Kinney, A. 1994, ApJ, 572, 581
Storchi-Bergmann, T., Rodriguez-Ardila, A., Schmitt, H. R., Wilson, A. S., & Baldwin, J. A. 1996, ApJ, 472, 83
Storchi-Bergmann, T., González Delgado, R. M., et al. 2001, ApJ, 559, 147
Storchi-Bergmann, T., Dors, O. L., Riffel, R. A., et al. 2007, ApJ, 670, 959
Viironen, K., Delgado-Inglada, G., Mampaso, A., Magrini, L., & Corradi, R. L. M. 2007, MNRAS, 381, 1719
Vilchez, J. M., & Pagel, B. E. J. 1988, MNRAS, 231, 257
Wakamatsu, K., & Nishida, M. T. 1980, PASJ, 32, 389